Science Advances
AAAS

advances.sciencemag.org/cgi/content/full/6/5/eaay4458/DC1

Supplementary Materials for

Molecular mechanism of SHP2 activation by PD-1 stimulation

M. Marasco, A. Berteotti, J. Weyershaeuser, N. Thorausch, J. Sikorska, J. Krausze, H. J. Brandt, J. Kirkpatrick, P. Rios, W. W. Schamel, M. Köhn*, T. Carlomagno*

*Corresponding author. Email: teresa.carlomagno@oci.uni-hannover.de (T.C.); maja.koehn@bioss.uni-freiburg.de (M.K.)

Published 31 January 2020, *Sci. Adv.* **6**, eaay4458 (2020)
DOI: 10.1126/sciadv.aay4458

This PDF file includes:

Supplementary Figures

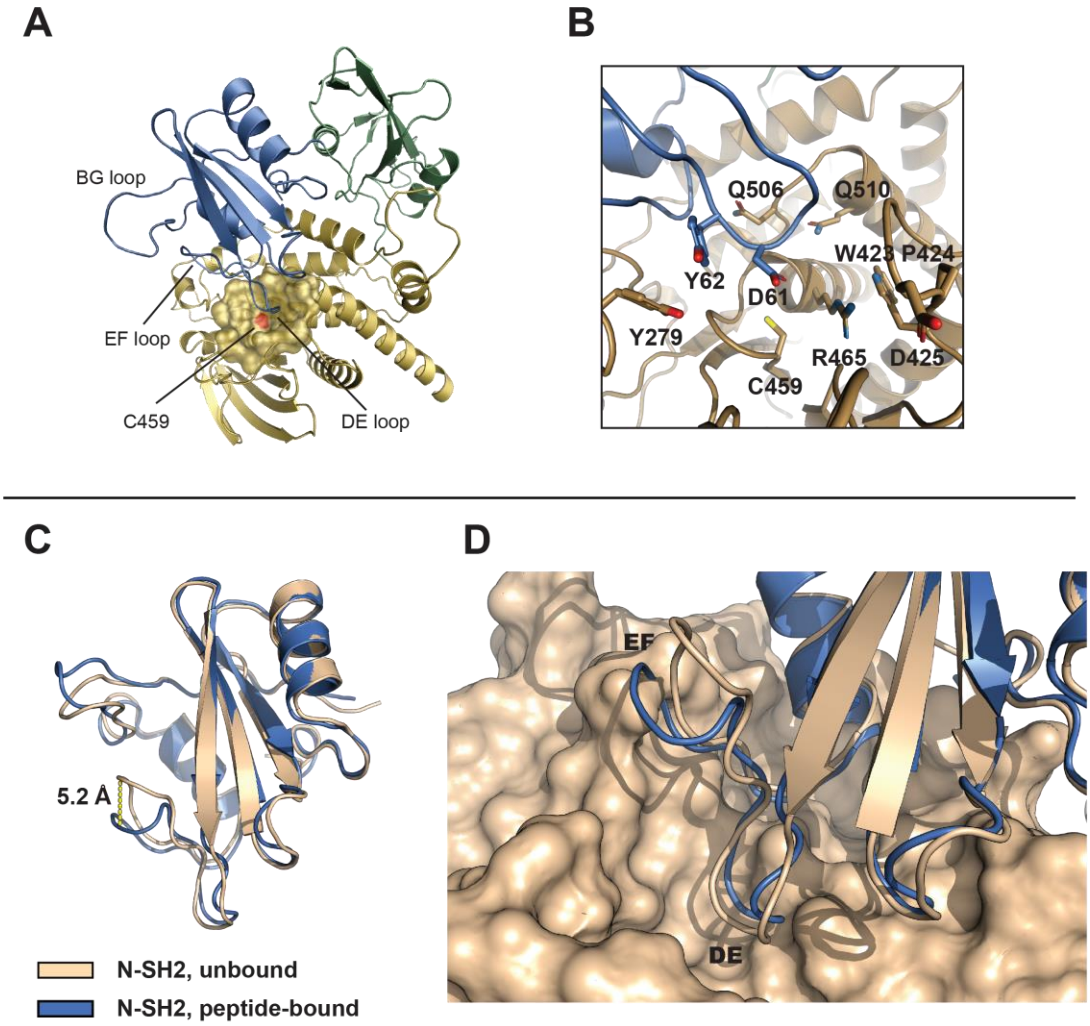

Fig. S1. Autoinhibited conformation of SHP2. (**A**) Structure of SHP2 as seen in PDB entry 2SHP. N-SH2 ($SHP2^{1-105}$): blue; C-SH2 ($SHP2^{110-220}$): green; PTP: yellow. The DE loop of N-SH2 occludes the catalytic site of PTP. The catalytic cysteine C459 is shown in red. (**B**) Detailed view of the catalytic pocket of the PTP domain occupied by the DE loop of N-SH2. (**C**–**D**) Conformational change of the N-SH2 domain upon phosphopeptide binding. (C) Overlay of the structure of unbound N-SH2 (ivory, PDB entry 2SHP) and phosphopeptide-bound N-SH2 (PDB entry 6ROZ, blue), showing the conformational change of the EF and BG loops. (D) Same as in (C) with the addition of the surface representation of the PTP domain, as in PDB entry 2SHP. The conformation of the EF loop of the N-SH2 domain when bound to phosphopeptides is incompatible with the relative orientation of the N-SH2 and PTP domains seen in PDB entry 2SHP, as evident from the steric clash of the EF loop with the surface of PTP.

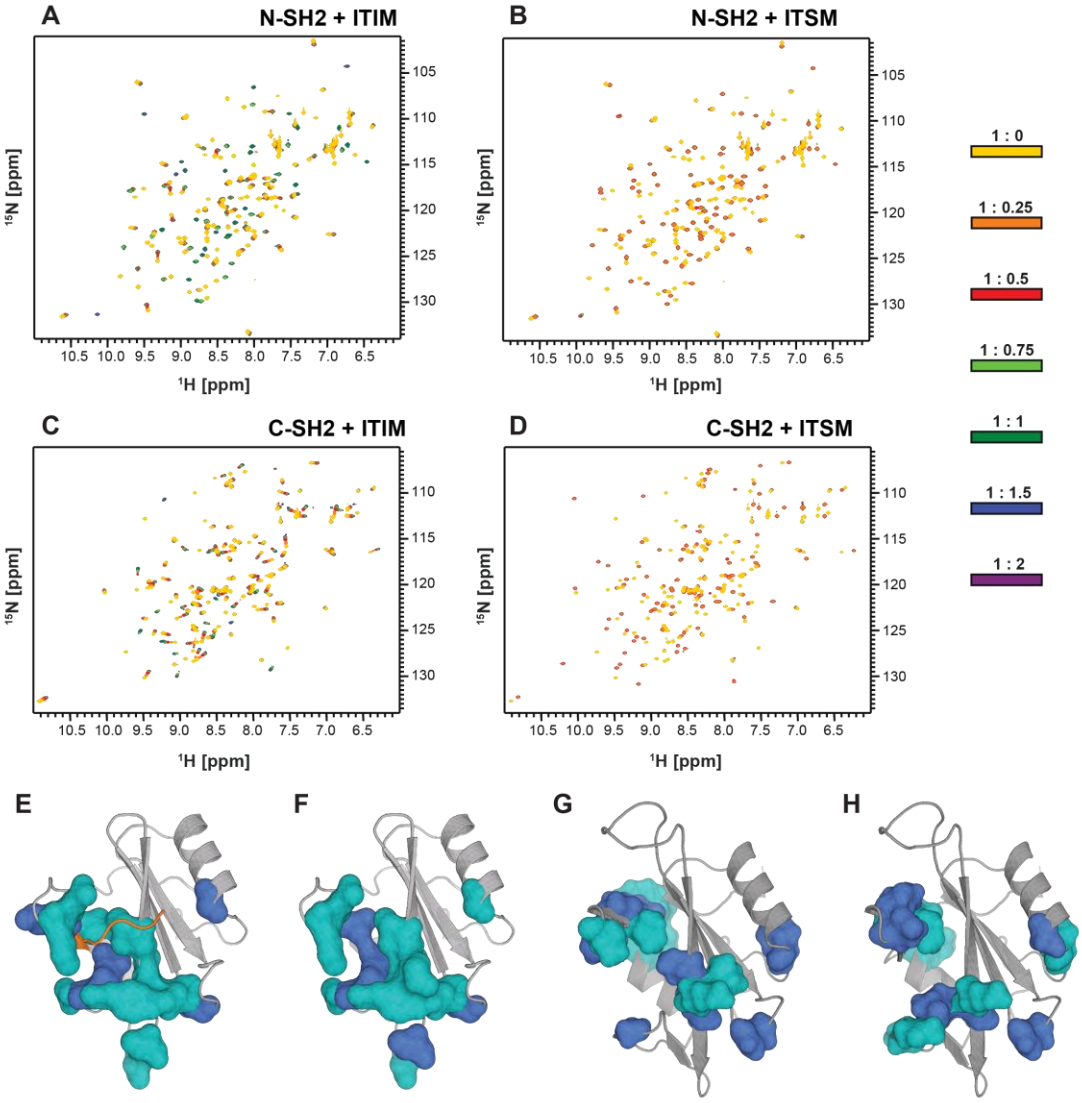

Fig. S2. Interaction of the N-SH2 and C-SH2 domains with ITIM and ITSM. The full ^{1}H-^{15}N spectra corresponding to the excerpts shown in Fig. 1 B–E. (**A**–**B**) ^{1}H-^{15}N spectra of N-SH2 upon addition of phosphorylated ITIM (A) and ITSM (B). (**C**–**D**) ^{1}H-^{15}N spectra of C-SH2 upon addition of phosphorylated ITIM (C) and ITSM (D). The protein concentration was 0.3-0.8 mM; the color-code on the side indicates the protein:peptide molar ratios. All spectra were recorded at 298 K and at 600 MHz. (**E**–**H**) Representation of the CSPs observed for N-SH2 in complex with either ITIM (E) or ITSM (F) and for C-SH2 in complex with either ITIM (G) or ITSM (H). The CSPs are color-coded depending on their size: blue: CSPs > average + 2 SD; cyan: CSPs > average + 1 SD; SD: standard deviation calculated over the CSPs of all residues in the respective protein. The structures of N-SH2 (E, F) are from PDB entry 5DF6; those of the C-SH2 (G, H) are from PDB entry 2SHP. In E the phosphopeptide

KFMPPTYTEVD from TXNIP (thioredoxin-interacting protein) is shown bound to N-SH2, as observed in PDB entry 5DF6.

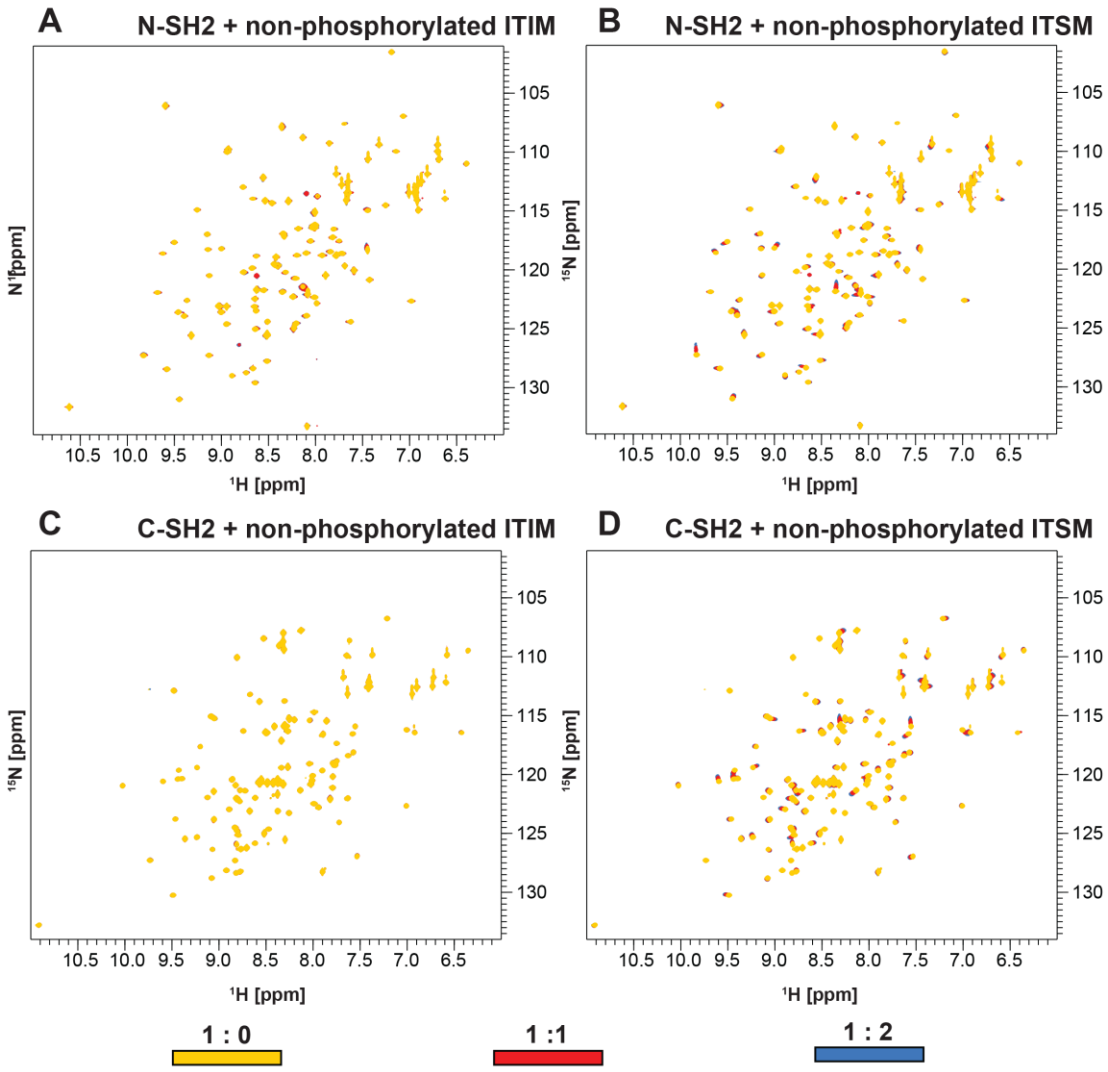

Fig. S3. Lack of phosphorylation on ITIM and ITSM severely impairs their ability to bind both N-SH2 and C-SH2. (**A–D**) ^{1}H-^{15}N spectra of N-SH2 upon addition of non-phosphorylated ITIM (A) and ITSM (B) or of C-SH2 upon addition of non-phosphorylated ITIM (C) and ITSM (D). The protein concentration was 0.3-0.8 mM; the color-code on the bottom indicates the protein:peptide molar ratios. No chemical shift perturbations were observed for non-phosphorylated ITIM, indicating that it binds neither N-SH2 nor C-SH2. The non-phosphorylated ITSM peptide binds both SH2 domains but with much reduced affinity compared to the phosphorylated peptide. All spectra were collected at 298 K and 600 MHz.

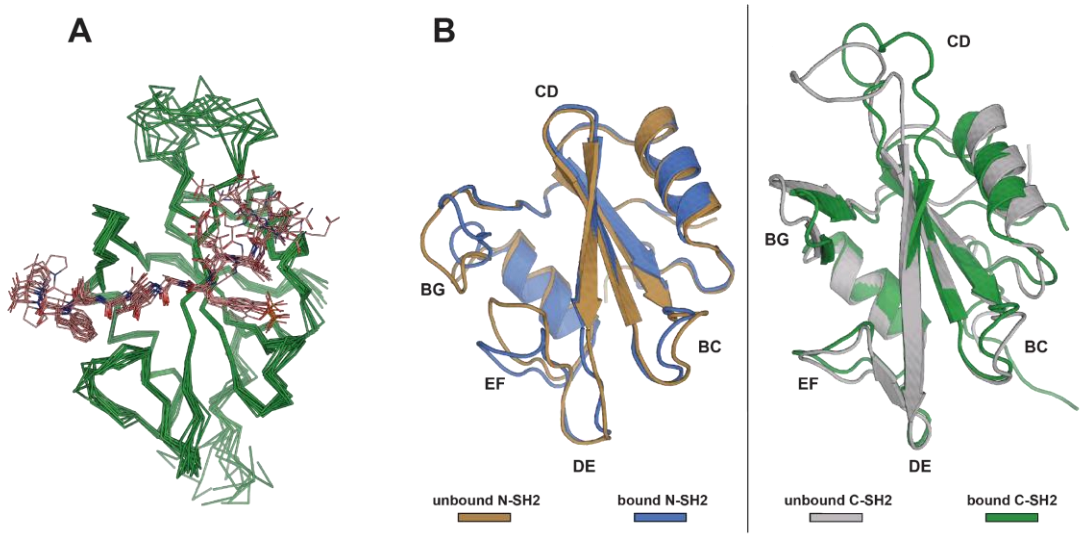

Fig. S4. NMR structure of the C-SH2–ITSM complex and overlay of unbound and phosphopeptide-bound structures of the SH2 domains. (**A**) NMR structure of the C-SH2–ITSM complex. Overlay of the 10 lowest-energy structures of the SHP2 C-SH2 domain in complex with ITSM, as determined by NMR spectroscopy. The details of the structure determination are given in Methods; the structural statistics and quality measures are given in Table S2. (**B**) Overlay of unbound and phosphopeptide-bound structures of the SH2 domains. Left, the structure of unbound N-SH2 from PDB entry SHP2 (gold) overlaid with the structure of N-SH2 in complex with ITSM (blue, PDB entry 6ROZ). The protein loops are labeled. The change in the conformations of the EF and BG loops is evident. Right, the structure of unbound C-SH2 from PDB entry SHP2 (grey) overlaid with the structure of C-SH2 in complex with ITSM (green, PDB entry 6R5G). In the unbound C-SH2 domain, the conformation of the EF loop is already in the peptide-bound form.

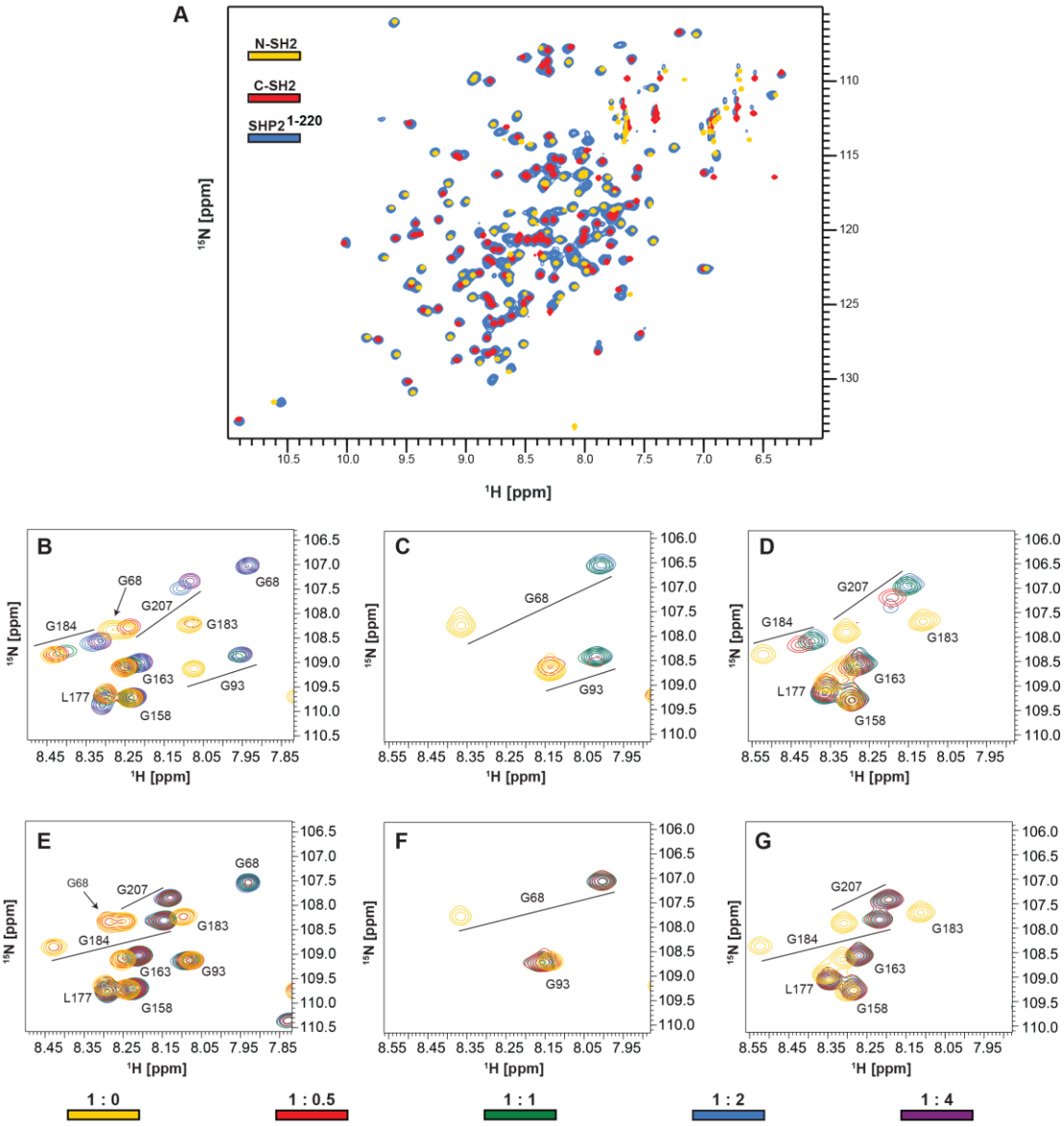

Fig. S5. Overlay of the ^{1}H-^{15}N spectra of SHP2$^{1–220}$, SHP2$^{1–105}$, and SHP2$^{110–220}$ in the bound and unbound forms. (**A**) The close overlap of the NMR resonances of SHP2$^{1-220}$, N-SH2 and C-SH2 domains, shows that in the SHP2$^{1-220}$ construct, the two SH2 domains do not interact with each other to a significant extent. SHP2$^{1-220}$: blue; SHP2$^{1-105}$ (N-SH2): yellow; SHP2$^{110-220}$ (C-SH2): red. (**B**–**D**) ^{1}H-^{15}N spectra of SHP2$^{1-220}$ (B), N-SH2 (C) and C-SH2 (D) in the presence of increasing concentrations of ITIM. The CSP pattern of SHP2$^{1-220}$ (B) reproduces those of the isolated N-SH2 (C) and C-SH2 (D) domains. (**E**–**G**) ^{1}H-^{15}N spectra of SHP2$^{1-220}$ (E), N-SH2 (F) and C-SH2 (G) in the presence of increasing concentrations of ITSM. The CSP pattern of SHP2$^{1-220}$ (E) reproduces those of the isolated N-SH2 (F) and C-SH2 (G) domains.

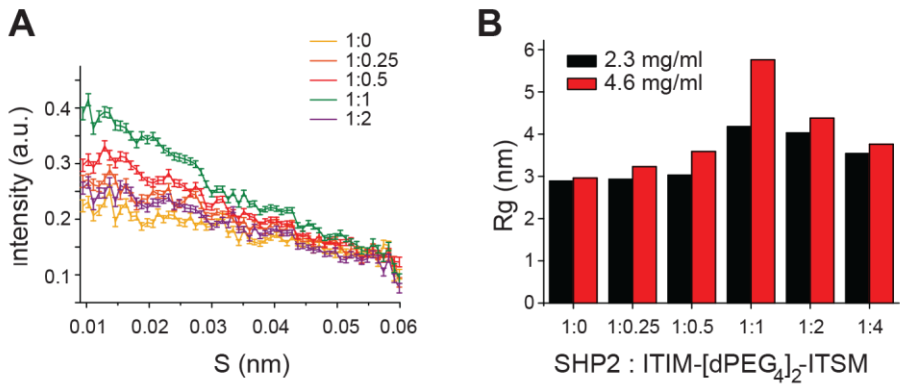

Fig. S6. Small-angle scattering analysis of SHP2$^{1–220}$ and SHP2$^{1–525}$-C459S in the presence of the bidentate peptide. (**A**) Small Angle Neutron Scattering (SANS) curves of SHP2$^{1-220}$ measured at KWS-1 (Heinz Meier – Leibniz Zentrum, Munich, Germany), using a sample-detector distance of 8 and 1.5 m, collimation length of 8 m and neutron wavelength (λ) of 5 Å. The protein samples were perdeuterated and dissolved in 100 mM MES (2-(N-morpholino)ethanesulfonic acid), 150 mM NaCl, 5 mM DTT, pH 6.8 with a D_2O:H_2O ratio of 0.42. The temperature for the measurements was set to 20 °C. The protein concentration was 190 µM (4.75 mg/ml). The initial slope of the SANS curve represents the radius of gyration (R_g) of SHP2$^{1-220}$, as the scattering density of the non-perdeuterated peptide is matched by the solvent at the D_2O:H_2O ratio of 0.42. The SHP2$^{1-220}$ R_g increases steadily up to a protein:peptide molar ratio of 1:1, indicating the formation of oligomers bridged by the bidentate peptide, and decreases again at lower protein:peptide molar ratios, as the oligomers are dissolved in favour of protein:peptide complexes with a 1:2 stoichiometry. (**B**) Radii of gyration derived from the Small Angle X-ray Scattering (SAXS) data (Guinier analysis) of SHP2$^{1-525}$-C549S collected at the ESRF BioSAXS beamline BM29 (Grenoble, France). The samples were measured at 20 °C in 50 mM HEPES, 150 mM NaCl, 5 mM DTT, pH 7.6 for two protein concentrations. As for SHP2$^{1-220}$, the radius of gyration of SHP2$^{1-525}$ increases in the presence of the bidentate peptide up to a protein:peptide molar ratio of 1:1, and decreases again at lower molar ratios, as the oligomers are dissolved in favour of protein:peptide complexes with a 1:2 stoichiometry. Lower concentrations of SHP2$^{1-525}$ lead to less multimeric species as suggested by the lower R_g values.

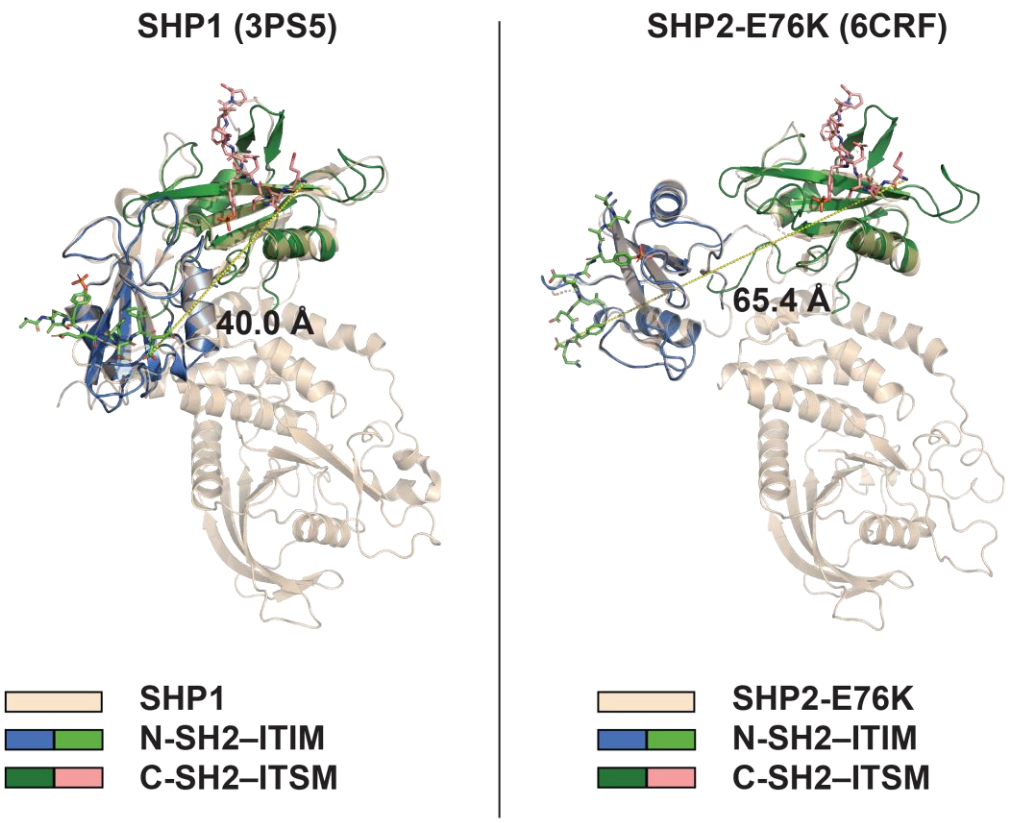

Fig. S7. Superposition of the structures of N-SH2–ITIM and C-SH2–ITSM on the corresponding domains of SHP1 in the open state (PDB entry 3PS5) and SHP2-E76K in the open state (PDB entry 6CRF). The position of the N-SH2 domain differs in the two structures. The structure of SHP1 is compatible with the simultaneous binding ITIM and ITSM of the PD-1-derived bidentate peptide to the N-SH2 and C-SH2 domains, respectively (linker length ~40 Å), while the structure of SHP2-E76K is not.

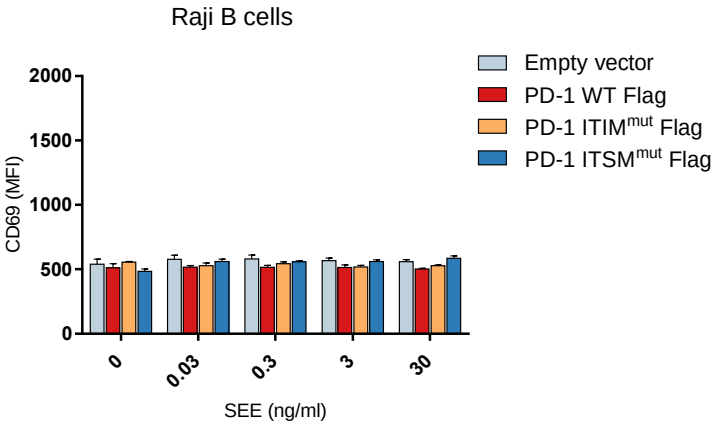

Fig. S8. CD69 expression levels of Raji B cells are not affected by coculture with Jurkat T cells. CD69 expression levels of superantigen (SEE)-loaded Raji B cells were not affected by co-culture with the indicated T cell lines (WT Flag, ITIM^{mut} Flag, ITSM^{mut} Flag). CD69 expression was measured by flow cytometry. The mean fluorescent intensity (MFI) is shown. Data points represent one out of three independent experiments, each performed in triplicate.

Supplementary Tables

Table S1. Crystallographic data collection and refinement statistics.

	N-SH2–ITSM	N-SH2–ITIM
Data collection		
Space group	$P4_3$	$P4_3$
Cell dimensions		
a, *b*, *c* (Å)	30.03, 30.03, 213.11	28.86, 28.86, 208.23
α, β, γ (°)	90.0, 90.0, 90.0	90.0, 90.0, 90.0
Resolution (Å)	42.62-2.89 (3.07-2.89)	41.65-2.10 (2.16-2.10)
R_{merge}	0.0182 (1.316)	0.192 (1.149)
I / σI	10.4 (2.0)	11.2 (2.0)
Completeness (%)	100.0 (100.0)	100.0 (100.0)
Redundancy	13.8 (13.2)	13.8 (12.8)
*CC*1/2	0.998 (0.764)	0.946 (0.526)
Refinement		
Resolution (Å)	30.03-2.89 (2.99-2.89)	29.86-2.10 (2.18-2.10)
No. reflections	4,218 (455)	10,548 (1,035)
R_{work} / R_{free}	0.2394 / 0.2846	0.2253 / 0.2785
No. atoms		
Protein	1,808	1,796
Ligand/ion	0	0
Water	0	26
B-factors (Å^2)		
Protein	71.0	35.2
Ligand/ion	-	-
Water	-	20.1
R.m.s. deviations		
Bond lengths (Å)	0.009	0.009
Bond angles (°)	1.25	1.38

Values in parentheses are for the highest-resolution shell. Each dataset was collected from a single crystal.

Table S2. NMR statistics for the structure of the C-SH2–ITSM complex.

	C-SH2–ITSM
NMR distance and dihedral restraints	
Distance restraints	
Total NOE	6108
Intra-residue	1642
Inter-residue	
Sequential ($\|i - j\| = 1$)	1383.7
Medium-range ($\|i - j\| \leq 4$)	921.3
Long-range ($\|i - j\| > 5$)	1937.5
Intermolecular	223.5
Hydrogen bonds	0
Dihedral angle restraints	
φ	95
ψ	95
Structure statistics	
Violations (mean and SD)	
Distance restraints (Å)	>0.5 Å: 0 (+/– 0) >0.3 Å: 1.9 (+/– 1.44) >0.1 Å: 58.3 (+/– 2.97)
Dihedral angle restraints (º)	>10°: 0 (+/– 0) >5°:0.8 (+/– 0.87)
Max. dihedral angle violation (º)	5.7
Max. distance constraint violation (Å)	0.38
Deviations from idealized geometry	
Bond lengths (Å)	4.2E-03 (+/– 1.18E-04)
Bond angles (º)	0.59 (+/– 9.9E-02)
Impropers (º)	1.49 (+/– 4.5E-02)
Average pairwise RMS deviation** (Å)	
Heavy	0.96 +/– 0.11
Backbone	0.38 +/– 0.06

** Pairwise RMS deviation was calculated over the 10 water-refined structures.